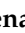





## Article

# Effectiveness and Compatibility of Nanoparticle Based Multifunctional Coatings on Natural and Man-Made Stones

Martina Zuena <sup>1</sup>, Ludovica Ruggiero <sup>1</sup>, Giancarlo Della Ventura <sup>1</sup>, Edoardo Bemporad <sup>2</sup>,  
Maria Antonietta Ricci <sup>1</sup> and Armida Sodo <sup>1,\*</sup>

<sup>1</sup> Dipartimento di Scienze, Università Degli Studi Roma Tre, Via della Vasca Navale 84, 00146 Roma, Italy; martina.zuena@uniroma3.it (M.Z.); ludovica.ruggiero@uniroma3.it (L.R.); giancarlo.dellaventura@uniroma3.it (G.D.V.); mariaantonia.ricci@uniroma3.it (M.A.R.)

<sup>2</sup> Dipartimento di Ingegneria, Università Degli Studi Roma Tre, Via della Vasca Navale 79, 00146 Rome, Italy; edoardo.bemporad@uniroma3.it

\* Correspondence: armida.sodo@uniroma3.it

**Abstract:** The interaction of microorganisms with stone materials leads to biodeterioration processes, which may cause aesthetic damages and the loss of durability and strength of the substrates. Innovative solutions against this process are represented by nanotechnologies. In our previous works, 2-mercaptobenzothiazole was successfully encapsulated within two silica-based nanodevices: nanocapsules and mesoporous nanoparticles. Such loaded nanodevices have been dispersed in TEOS based coatings, characterized as far as their chemical–physical properties and in vitro biocide efficacy. Here, we adopt a multi-technic approach, to assess the coatings efficacy and compatibility with four types of stones of cultural heritage interest, namely, mortar, brick, travertine, and Carrara marble. In particular, we determine the protective function of the coatings, based on water transport properties (reduction up to a factor 10 of the water absorption for brick and mortar, without significantly influencing water vapor transmission rate), morphology of the surface (absence of coating cracks and color changes), and TiO<sub>2</sub> photocatalytic activity. Consequently, these coatings can be considered suitable for application on stone artifacts, without interfering with their artistic appearance.

**Keywords:** stone protection; multifunctional coatings; Si nanocontainers; TiO<sub>2</sub> nanoparticles



**Citation:** Zuena, M.; Ruggiero, L.; Della Ventura, G.; Bemporad, E.; Ricci, M.A.; Sodo, A. Effectiveness and Compatibility of Nanoparticle Based Multifunctional Coatings on Natural and Man-Made Stones.

*Coatings* **2021**, *11*, 480. <https://doi.org/10.3390/coatings11040480>

Academic Editor:  
Jean-François Berret

Received: 29 March 2021  
Accepted: 17 April 2021  
Published: 20 April 2021

**Publisher's Note:** MDPI stays neutral with regard to jurisdictional claims in published maps and institutional affiliations.



**Copyright:** © 2021 by the authors. Licensee MDPI, Basel, Switzerland. This article is an open access article distributed under the terms and conditions of the Creative Commons Attribution (CC BY) license (<https://creativecommons.org/licenses/by/4.0/>).

## 1. Introduction

Both natural and man-made stone materials, used in the field of cultural heritage, undergo a weathering process of deterioration when exposed to outdoor conditions. The presence of water and salts, atmospheric pollution, and microorganisms colonizing the porous structure of the stone, are the most frequent degradation agents [1–5]. In particular, the chemical and physical interactions between the stone support and the biodeteriogens (such as bacteria, fungi, and algae) can cause both mechanical and aesthetical damages.

Bioremediation treatments are applied to remove the biological patina and to inhibit its recurrence. An effective treatment must be non-toxic and compatible with the treated substrates [6]. The common approach against biodeterioration is the direct application on the stone surface of biocides as such or diluted into coating formulations. However, biocides are usually toxic and can be subject to environmental stresses, due to temperature excursion, UV radiation, and rains, leading to a reduced efficacy [7–10]. Consequently, these interventions need frequent re-applications (every 6 months–one year), implying relevant costs for private and public sectors [6]; thus, requiring the search for an innovative approach. Encapsulation of biocides into nanocontainers dispersed in a coating formulation can be a good strategy for managing the release of the biocide compounds, reducing, at the same time, their environmental degradation and toxic effects [11–14].

With this aim, we encapsulated a commercial biocide (2-mercaptobenzothiazole, MBT) and a natural product antifoulant (zosteric sodium salt) into two different silica nanocon-

tainers, namely core-shell nanocapsules (NC) and mesoporous nanoparticles (MNP) [11,15]. The charged nanoparticles were successfully characterized with respect to their dimensions, superficial properties, loading/release, and in-vitro antifouling capability in a previous work [11].

The nanocontainers were then diluted in a TEOS matrix with the addition of TiO<sub>2</sub> nanoparticles as photocatalytic agent. Since TEOS-based coatings undergo cracking during the drying phase [16–18], we tried to improve the formulation by the addition of poly(dimethylsiloxane) hydroxyl-terminated (PDMS-OH) and n-octylamine. In fact, PDMS-OH is known to improve the coating elasticity, thus reducing cracking due to the capillary pressure [19]. Moreover, n-octylamine increases coating porosity, thus contributing to the dissipation of internal tensions, and catalyzing TEOS polymerization, improving its adhesion with carbonate stone materials [20–22]. Our formulation, when silica nanodevices and TiO<sub>2</sub> nanoparticles weight percentage is of the order of 0.1%, is transparent, does not show cracks, and does not modify the color of the coating. Furthermore, it dries more slowly than the empty coating, allowing a deeper penetration inside the pores of a treated surface [22].

Given these promising results on chemical–physical characterization of the coating, here we investigated its interaction with four stone supports commonly used as construction materials in cultural heritage.

In detail, we present the mechanical and colorimetric characterization of the synthesized multifunctional coating containing MBT (loaded in two different nanodevices), applied on four stone materials characterized by different porosity, namely natural hydraulic lime mortar, brick, travertine, and Carrara marble.

A multi-analytical approach was used to investigate the performances of the coating and, in particular, to assess its behavior as a consolidant or a protective product. This was done by evaluating changes in water wetting and transport properties, lithotype surface color, coating morphology, and penetration depth. The photocatalytic activity due to the presence of TiO<sub>2</sub> nanoparticles was evaluated both in the laboratory and in-situ, namely in a sunny area of the garden of the Science Department of Roma Tre University. Finally, the antifouling properties of the coatings applied directly on the stone have been under study, by considering one year as monitoring period.

## 2. Materials and Methods

### 2.1. Coating Formulation

Following reference [11], we used acetyltrimethylammonium bromide (CTAB, Aldrich, St. Louis, MO, USA), ammonia solution (NH<sub>3</sub> aq. 30%, Aldrich, St. Louis, MO, USA), diethyl ether (Et<sub>2</sub>O, Aldrich, St. Louis, MO, USA), tetraethoxysilane (TEOS, Aldrich, St. Louis, MO, USA), and 2-mercaptobenzothiazole (MBT, Sigma-Aldrich, St. Louis, MO, USA) for the synthesis of the loaded nanocontainers. The characteristics of the obtained nanocontainers loaded with MBT are reported in Table 1.

**Table 1.** Characteristics of silica nanocontainers and TEOS-based coatings. NC: silica nanocapsules; MNP: silica mesoporous nanoparticles. Si-Control, coating without nanoparticles; Si-TiO<sub>2</sub>-NC: coating with silica nanocapsules and TiO<sub>2</sub> nanoparticles; Si-TiO<sub>2</sub>-MNP: coating with silica mesoporous nanoparticles and TiO<sub>2</sub> nanoparticles.

Samples	Morphology	Diameter (nm)	Loading Capability (Weight %)	Surface Area (m <sup>2</sup> /g)
NC	Spherical	140 ± 20	10	-
MNP	Spherical	39 ± 4	8.2	-
Si-Control	-	-	-	440
Si-TiO <sub>2</sub> -NC	-	-	-	489
Si-TiO <sub>2</sub> -MNP	-	-	-	488

For the coating preparation, TiO<sub>2</sub> nanoparticles (Sigma-Aldrich, St. Louis, MO, USA, with an average particle size of ~21 nm), TEOS, ethanol (Carlo Erba Reagents S.r.l., Cornaredo, Italy), poly(dimethylsiloxane) hydroxyl-terminated (PDMS-OH, Sigma-Aldrich,

St. Louis, MO, USA), and a non-ionic surfactant (n-octylamine, Sigma-Aldrich, St. Louis, MO, USA) were used. All compounds were employed without any further purification. The synthesis protocol was reported in a recent paper [23]. The used mole ratios were 1TEOS/16Ethanol/10H<sub>2</sub>O/0.04PDMS-OH/0.004 n-octylamine. Briefly, two distinct sols were obtained by mixing TEOS, ethanol, TiO<sub>2</sub> nanoparticles, and either loaded NC or MNP silica nanoparticles. The total nanoparticle concentration was set at 0.1% *w/w* to achieve optimal results, in terms of porosity, optical properties, and lack of cracking, according to previous results [22].

The nanoparticle-charged coatings were applied on the selected lithotypes. For each substrate, a control sample treated with the coating alone without nanoparticles was prepared. The tested coatings were hereafter labeled as: Si-TiO<sub>2</sub>-NC (coating with silica nanocapsules and TiO<sub>2</sub> nanoparticles), Si-TiO<sub>2</sub>-MNP (coating with silica mesoporous nanoparticles and TiO<sub>2</sub> nanoparticles), and Si-Control (coating without nanoparticles). The chemical composition, morphology, pore volume, and pore size distribution of the prepared coatings are reported in reference [22] and the surface area (m<sup>2</sup>/g) is reported in Table 1.

## 2.2. Stone Samples

Four different stone supports (5 × 5 × 1 cm<sup>3</sup>) were selected to evaluate the mechanical and colorimetric performances of the coating. A lime-based mortar (MO) was prepared by using natural hydraulic lime, NHL 5, provided by Saint Astier mixed with standard river sand aggregates (size <4 mm) in proportion of 1:2, adding water to achieve good workability. The mortar mixture was cured for 24 h at room conditions (RH% = 50%, 20 °C) and used for testing after 28 days. Red-fired bricks (BR) were purchased from a local wholesale. Travertine (TR), and Carrara marble (MA) were purchased directly from Tivoli and Carrara quarries, respectively. Both stones underwent an aging process (two heating cycles at 600 °C and storage in water overnight at room temperature [24]), in order to increase their porosity.

## 2.3. Coating Deposition

In order to reproduce the common procedure adopted in-situ by the restorers, the coatings were applied by brush until saturation, i.e., until the surface remained wet for more than 1 min. In particular, 16 applications were required for mortar and brick, 6 for Carrara marble, and 4 for travertine. The coatings were applied on the smallest surface (5 × 1 cm<sup>2</sup>) of each specimen in order to test water absorption through capillarity, and on the largest surface (5 × 5 cm<sup>2</sup>) for all other tests.

Curing of the coatings was achieved by drying at laboratory conditions (RH% = 50%, 20 °C) for 1 week until a constant mass was observed. The amount of applied product (kg/m<sup>2</sup>) was evaluated by weighting the samples before and immediately after each treatment, while the amount of dry matter retained (kg/m<sup>2</sup>) was evaluated by weighting the specimens before and one week after the treatment. These data are available in Tables S1 and S2 in Supplementary Materials.

## 2.4. Characterization Techniques

To evaluate the performances of the coating formulations, several laboratory tests were carried out. Static contact angle, water absorption through capillarity, and water vapor permeability were used to evaluate changes in water transport, stone wettability, and waterproofing properties of the coatings.

To evaluate the static contact angle, 10 drops of distilled water with a volume of 5 µL were deposited on the horizontal surface of each analyzed sample. After 10 s of contact, both right and left contact angle between each drop and surface were measured by a camera. The results were elaborated by AnalySIS Pro<sup>®</sup> 3.2 software (Soft Imaging System GmbH, Münster, Germany).

Water absorption through capillarity was performed according to the procedure reported in the normative UNI EN 15801:2010 [25]. The same samples were analyzed before and after the application of the treatments and the results were expressed as the average of three samples. Before the test, the stone samples were dried at 60 °C until a constant mass was measured. The test was carried out by placing the samples on a bedding layer of filter paper soaked with distilled water and by weighting the samples at time intervals. The capillary water absorption coefficient (CWAC) was obtained from the angular coefficient of the initial part of the capillary absorption curve, expressed as the quantity of water absorbed per area over time.

Water vapor permeability, reported as the water vapor permeability coefficient (g), was determined in accordance with the standard DIN 52 615 [26]. The stone samples were dried at 60 °C and then analyzed before and after the application of the treatments. The results are reported as the average of three samples. The specimens were anchored on a squared iron container to expose the largest coated surface to the 93% internal relative humidity, obtained by a saturated aqueous solution of KNO<sub>3</sub> [27]. These container-specimen systems were placed in a room with constant relative humidity (50%) and temperature (20 °C). Their weights were monitored every 24 h until stability.

Colorimetric analysis was performed to evaluate the optical compatibility of the coatings. According to the NORMAL 43/93 [28], the color difference ( $\Delta E^*$ ) due to the coatings application with respect to the untreated stones, was expressed in the CIEL<sup>\*</sup>*a*<sup>\*</sup>*b*<sup>\*</sup> space according to Formula (1):

$$\Delta E = \sqrt{\Delta L^{*2} + \Delta a^{*2} + \Delta b^{*2}} \quad (1)$$

where  $L^*$  is the lightness, while  $a^*$  and  $b^*$  are the colorimetric coordinates for the red/green parameters and the yellow/blue ones, respectively ( $a^* < 0$  green,  $a^* > 0$  red,  $b^* < 0$  blue and  $b^* > 0$  yellow). The colorimetric variations ( $\Delta L^*$ ,  $\Delta a^*$ ,  $\Delta b^*$ ) were obtained by comparing  $L^*$ ,  $a^*$ ,  $b^*$  values achieved from untreated and treated specimens. Color were acquired with an Eoptis CLM-194 portable colorimeter (Trento, Italy), in the following conditions: illuminant D65 and observer 2°. The measurement area is a circle of 10 mm diameter, and the results are reported with the specular component included (SCI). Data were acquired on three samples for each coating and three points per sample, before and after treatment. The measurements of treated samples were performed 1 month after the coating application. The threshold of  $\Delta E^* = 5$  was adopted as the limiting value above which the color variation was visible by the naked eye [29,30].

Optical surface roughness (OSR) and scanning electron microscopy-energy dispersive X-ray spectroscopy (SEM-EDS) analysis were used to visualize surface morphological and physical inhomogeneities. Moreover, SEM-EDS was employed to investigate the distribution of the coating, both on the surface and in-depth.

OSR analysis was carried out with a confocal Leica DCM 3D optical profilometer (Leica Microsystems, Wetzlar, Germany). The analyzed parameter is  $R_z$ , which defines the average differences between the maximum peak height and the maximum peak valley depth within the sampling length [31]. A total of 500 profiles were recorded in the Z direction for each sample over an area of 5 × 5 mm<sup>2</sup> with a resolution along the axis of 2.5 μm. Measurements were performed on three points per sample, on both treated and untreated specimens: the results are expressed as the average of the obtained values.

Scanning Electron Microscopy (SEM) images were obtained with a Zeiss Sigma 300 (Oberkochen, Germany) from surface fragments of treated and untreated specimens, sputter-coated with gold. Morphological images were collected with an ETSE (Everhart-Thornley secondary electron) detector. XRF (X-ray fluorescence) chemical maps were acquired with a 60 mm<sup>2</sup> Bruker high-resolution EDS (energy dispersive X-ray, Berlin, Germany) detector; the scanned area was ~2400 μm<sup>2</sup>.

The preservation of the photocatalytic properties of TiO<sub>2</sub> nanoparticles within the coatings was tested by measuring the photocatalytic degradation of methyl orange. These tests have been performed at laboratory conditions, according with literature [21], and

in-situ, in a sunny area of the garden of Science Department of Roma Tre (Roma, Italy). Coated and untreated stone samples were covered with a solution of 1 mM of methyl orange (Riedel-de Haën, Seelze, Germany) in ethanol: 750  $\mu$ L for mortar and brick, and 500  $\mu$ L for travertine and Carrara marble, respectively, because of their different absorption coefficients. In addition, two control samples were tested, one untreated (NT) and another treated with a coating containing only titanium nanoparticles (Si\_TiO<sub>2</sub>). In the laboratory test, all samples were located in a ventilated chamber and irradiated for 72 h with 365 nm UV light (Osram vitalux, Berlin, Germany). The distance between the specimens and the lamp was set at 20 cm [21]. In-situ, all specimens were exposed to natural solar light over the month of November 2020. Photo degradation was evaluated by the same colorimeter quoted above. The color of the surfaces at time zero (without methyl orange) was taken as a reference for the discoloration curves and reported in Figure 5 after normalization to 100.

### 3. Results and Discussion

The effectiveness of the coatings in preventing water penetration and reducing water transport was evaluated by static contact angle, water absorption through capillarity, and water vapor permeability measurements.

Generally, the increase of hydrophobicity due to the presence of a polymer coating can be connected to the decrease of the contact area (and increase of contact angle) between the treated surface and the water droplets [32]. The results of the static contact angle analysis on the coated samples are reported in Table 2. All uncoated materials were superhydrophilic: in fact, the water drops were absorbed so quickly that the static contact angle could not be measured. All investigated coatings led to an increased hydro-repulsion and the presence of MNP or NC did not seem to significantly affect the performances of the treatment with respect to the pure coating, within the experimental uncertainty. Nevertheless, in the case of bricks, we noticed a better performance of the MNP/NC loaded coatings with respect to the pure coating. While in the case of mortar, NC loaded coatings provided better results, with respect to pure and MNP loaded ones. These results are the consequence of the higher porosity of brick and mortar compared to travertine and Carrara marble, while the different behavior of the Si\_TiO<sub>2</sub>-MNP coatings on brick and mortar may be due to the different pore sizes of the two materials.

**Table 2.** Average static contact angle for all samples after treatments.

Sample	Average Static Contact Angle (°)		
	Si_Control	Si_TiO <sub>2</sub> -NC	Si_TiO <sub>2</sub> -MNP
Brick	125.7 ± 4.7	143.4 ± 5.2	140.1 ± 5.5
Mortar	127.7 ± 3.5	140.1 ± 2.2	127.2 ± 3.9
Travertine	118.9 ± 5.1	119.7 ± 3.2	107.5 ± 5.5
Carrara Marble	125.5 ± 4.2	135.6 ± 2.9	128.6 ± 3.4

Si\_Control: coating without nanoparticles; Si\_TiO<sub>2</sub>-NC: coating with TiO<sub>2</sub> nanoparticles and loaded silica nanocapsules; Si\_TiO<sub>2</sub>-MNP: coating with TiO<sub>2</sub> nanoparticles and loaded silica mesoporous nanoparticles.

The increased surface hydrophobicity of the samples after coating application evidences the protective effect of these coatings.

Data regarding water absorption through capillarity are reported in Figure 1. For brick and mortar, since untreated and treated samples absorb very different amounts of water, we used two different scales for the Y-axis: the left-hand axis refers to the untreated samples (Figure 1a,b, black line), while the right-hand one refers to the treated samples (Figure 1a,b, green, red, and blue lines). We notice the different behavior of the four samples, as far as the final amount of absorbed water and the initial slope of the curves. For all treated samples, there was a reduction of the water absorption rate, most evident in the case of mortar and brick. Moreover, treated brick samples showed a reduction of absorbed water from  $\cong 19$  kg/m<sup>2</sup> to a value between 2 and 6 kg/m<sup>2</sup>, depending on the type of coating. Similarly, for mortar, we observed a reduction of absorbed water from  $\cong 10$  kg/m<sup>2</sup> to 0.5–1 kg/m<sup>2</sup>.

Smaller (although visible) differences were observed in the case of travertine and Carrara marble. In these cases, the quantity of absorbed water after  $250\text{ s}^{1/2}$  went from  $\cong 2.5\text{ kg/m}^2$  for the untreated samples to  $\cong 2\text{ kg/m}^2$  for the treated ones in the case of travertine, and from  $\cong 2\text{ kg/m}^2$  to  $\cong 1.9\text{ kg/m}^2$  in the case of Carrara marble, respectively.

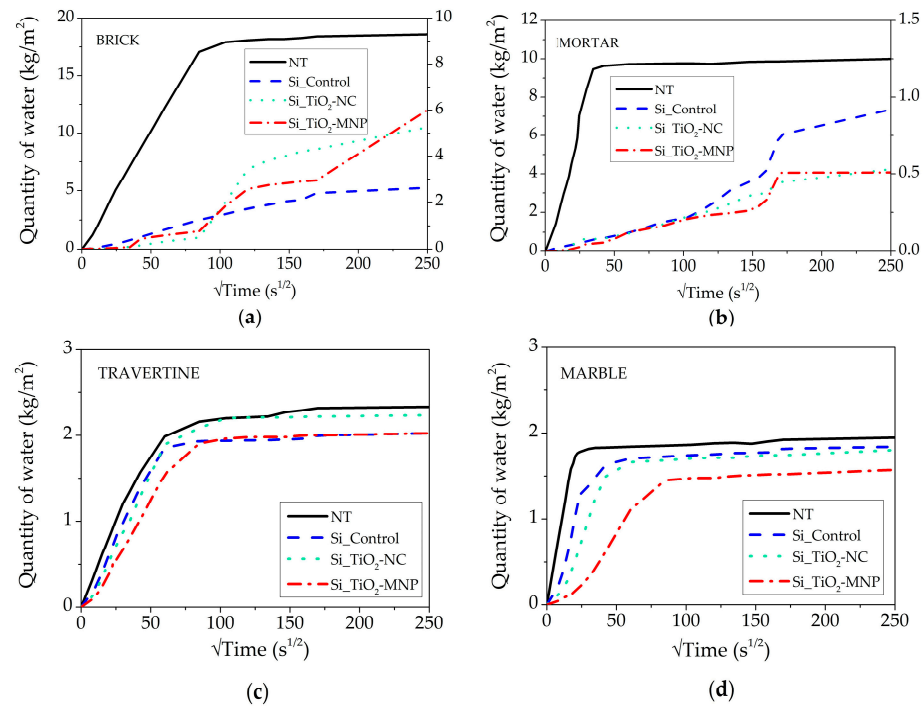


**Figure 1.** Quantity of water uptake versus time: (a) brick, (b) mortar, (c) travertine, and (d) Carrara marble. NT: untreated samples; Si\_Control: coating without nanoparticles; Si\_TiO<sub>2</sub>-NC: coating with TiO<sub>2</sub> nanoparticles and loaded silica nanocapsules; Si\_TiO<sub>2</sub>-MNP: coating with TiO<sub>2</sub> nanoparticles and loaded silica mesoporous nanoparticles. In the case of brick and mortar, data for Si\_Control, Si\_TiO<sub>2</sub>-NC, and Si\_TiO<sub>2</sub>-MNP refer to the right-hand axis scale. All other data refer to the left-hand axis scale.

Differences among the three coatings were not evident in general, with the exception of the case of Carrara marble, where the Si\_TiO<sub>2</sub>-MNP coating seemed to be more efficient. Further chemico-physical investigations are needed to confirm this finding. Finally, we evidenced a clear slope change of the curves relative to brick and mortar after about 100–170 s<sup>-1/2</sup>, while after the same time-lapse, travertine and Carrara marble reached saturation. This may be an artifact due to the water absorption through the lateral surfaces of the samples, not covered by the coating.

The described differences may be quantified by means of the capillary water absorption coefficient (CWAC), reported in Table 3. In the case of brick and mortar, we observed a reduction of CWAC larger than 90% for all applied coatings. Lower percentages were observed for travertine and Carrara marble, which are, by themselves, quite hydrophobic compared to the other two samples. Nevertheless, we noticed that the presence of the nanoparticles enhanced the stone hydro-repellence, with respect to the pure coating, and that a higher effect was observed for the coating containing MNP.

These results confirm the good performances of our coatings as protectants against water absorption.

On the other hand, a suitable protective product should limit water absorption without reducing (too much) the water vapor transmission rate. Figure 2 shows the water vapor permeability coefficient (g) for all samples, measured over one week: for each material, the direct comparison between the untreated (black) and treated sample is reported, by using different colors for the different materials. We stress that, due to the natural inhomogeneity

of the investigated materials, the  $g$  values of the untreated samples differ from one specimen to the other and, thus, the  $g$  value of each specimen before treatment is reported at the left hand side of its value after treatment. We observe that all treatments lead to a variation of  $g$  within the experimental uncertainties or, in the worst cases (brick treated with Si\_TiO<sub>2</sub>-NC and mortar treated with Si-TiO<sub>2</sub>-MNP) to a reduction smaller than 10%, which is, however, an acceptable variation [29]. Therefore, all investigated coatings, containing (or not) nanoparticles, do not significantly affect the natural behavior of the stones in terms of water vapor transport.

**Table 3.** Reduction (%) of the capillary water absorption coefficient (CWAC), due to the coating.

Sample	Reduction in CWAC (%)		
	Si_Control	Si_TiO <sub>2</sub> -NC	Si_TiO <sub>2</sub> -MNP
Brick	96.49	99.03	98.46
Mortar	98.97	99.28	99.46
Travertine	10.52	39.87	53.70
Carrara marble	46.25	57.47	86.21

Si\_Control: coating without nanoparticles; Si\_TiO<sub>2</sub>-NC: coating with TiO<sub>2</sub> nanoparticles and loaded silica nanocapsules; Si\_TiO<sub>2</sub>-MNP: coating with TiO<sub>2</sub> nanoparticles and loaded silica mesoporous nanoparticles.

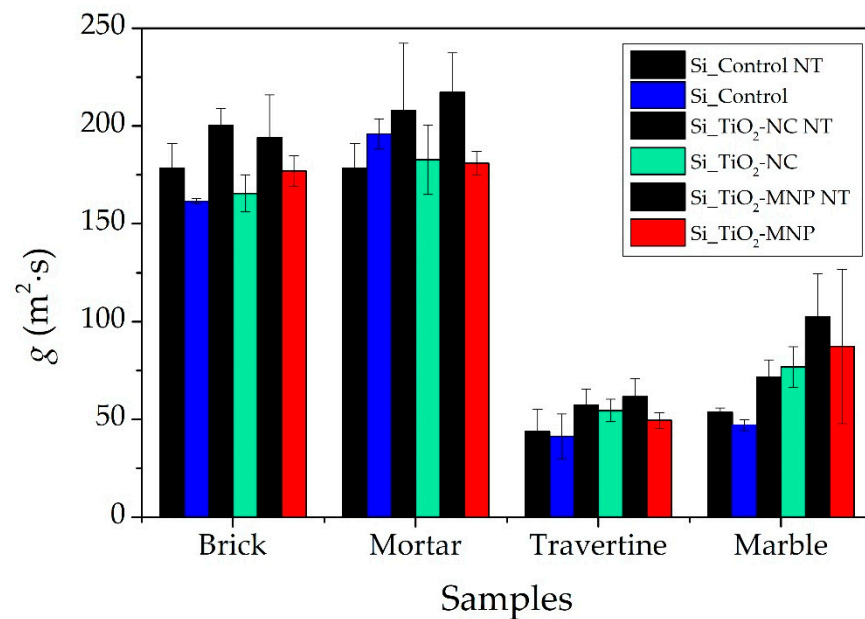


**Figure 2.** Water vapor permeability results expressed as water vapor permeability coefficient ( $g$ ), shown for the individual specimens before (black bar on the left) and after (colored bar on the right) treatment. In detail, all untreated samples (NT) are in black; Si\_Control: coating without nanoparticles; Si\_TiO<sub>2</sub>-NC: coating with TiO<sub>2</sub> nanoparticles and loaded silica nanocapsules; Si\_TiO<sub>2</sub>-MNP: coating with TiO<sub>2</sub> nanoparticles and loaded silica mesoporous nanoparticles.

The total color difference values ( $\Delta E^*$ ) of the samples, one month after the application of the coatings, are reported in Figure 3, while a more in-depth analysis of the colorimetric coordinates is given in Table S3, Supplementary material. All samples show  $\Delta E^* < 5$ , regardless of the type of treatment. Moreover, the differences with respect to the control sample are random, meaning that the presence of TiO<sub>2</sub> nanoparticles and silica nanocontainers do not modify the optical appearance of the stones. This demonstrates the validity of the coatings from an aesthetic point of view.

Changes in the morphology of the surface of the different samples after treatment have been investigated with optical surface roughness (OSR) and SEM analyses, in order

to verify if the good performance of the coatings, as far as cracking was concerned [22], was preserved after their application on the stones.

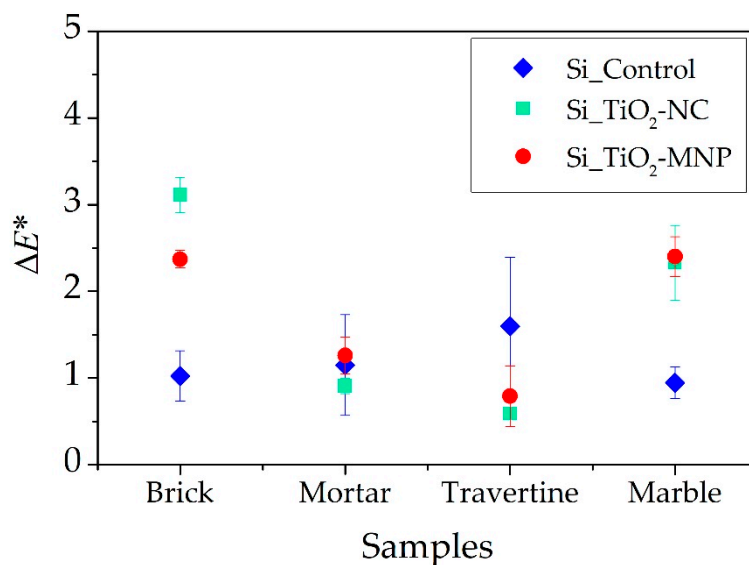


**Figure 3.** Color differences  $\Delta E^*$  generated by the application of all coatings, with respect to the untreated specimen: Si\_Control: coating without nanoparticles; Si\_TiO<sub>2</sub>-NC: coating with TiO<sub>2</sub> nanoparticles and loaded silica nanocapsules; Si\_TiO<sub>2</sub>-MNP: coating with TiO<sub>2</sub> nanoparticles and loaded silica mesoporous nanoparticles.

The OSR analyses (Figure S1 in Supplementary Materials) is expressed throughout the roughness profiles ( $R_z$ ), acquired along the  $x$ -axis, in order to determine the average height of surface irregularities. In most cases, no particular changes of roughness were observed after the application of the treatments, given the significant standard deviations on  $R_z$ .

SEM micrographs acquired from the surface treated with all coatings (Figure 4 and Figure S4b,d,f,h, Supplementary Material) show that all analyzed coatings are homogenous and crack-free. This demonstrates that our preparation recipe is effective in reducing the capillary pressure of the coating, responsible for possible cracking. Aggregations of nanoparticles are well evident, in particular on the surface of brick and mortar (see, in particular, Figure 4a–d), likely due to the higher number of applications required to obtain saturation. Moreover, SEM–EDS analysis allowed evaluating the distribution of the coatings, both on the surface and in-depth. This information was obtained by looking at the distribution of Ti and, in the case of travertine and Carrara marble, of Si (Figures S2 and S3, Supplementary Material). Si was not looked for in the case of brick and mortar since it is already abundant in the untreated material. The micrographs show a homogenous distribution of both Ti and Si on the surface of all treated stones, independently of the differences among the used coatings. Importantly, the cross-sections of the samples do not show the presence of Ti and Si under the sample surface, suggesting that the coatings do not penetrate deeply inside the material, confirming the protective (and not consolidant) function of the investigated products.

Finally, the photocatalytic property of TiO<sub>2</sub> nanoparticles added to the coating formulation was investigated, both under controlled conditions in the laboratory and in-situ. Laboratory measurements allow a better control of the photocatalytic property of the coating with respect to in-situ measurements, due to weather variability. In fact, the data obtained from the in-situ samples can be influenced by uncontrolled factors, such as humidity and dust: these are particularly relevant in the case of the most porous materials, such as bricks and mortars, and may affect the colorimetric measurement.



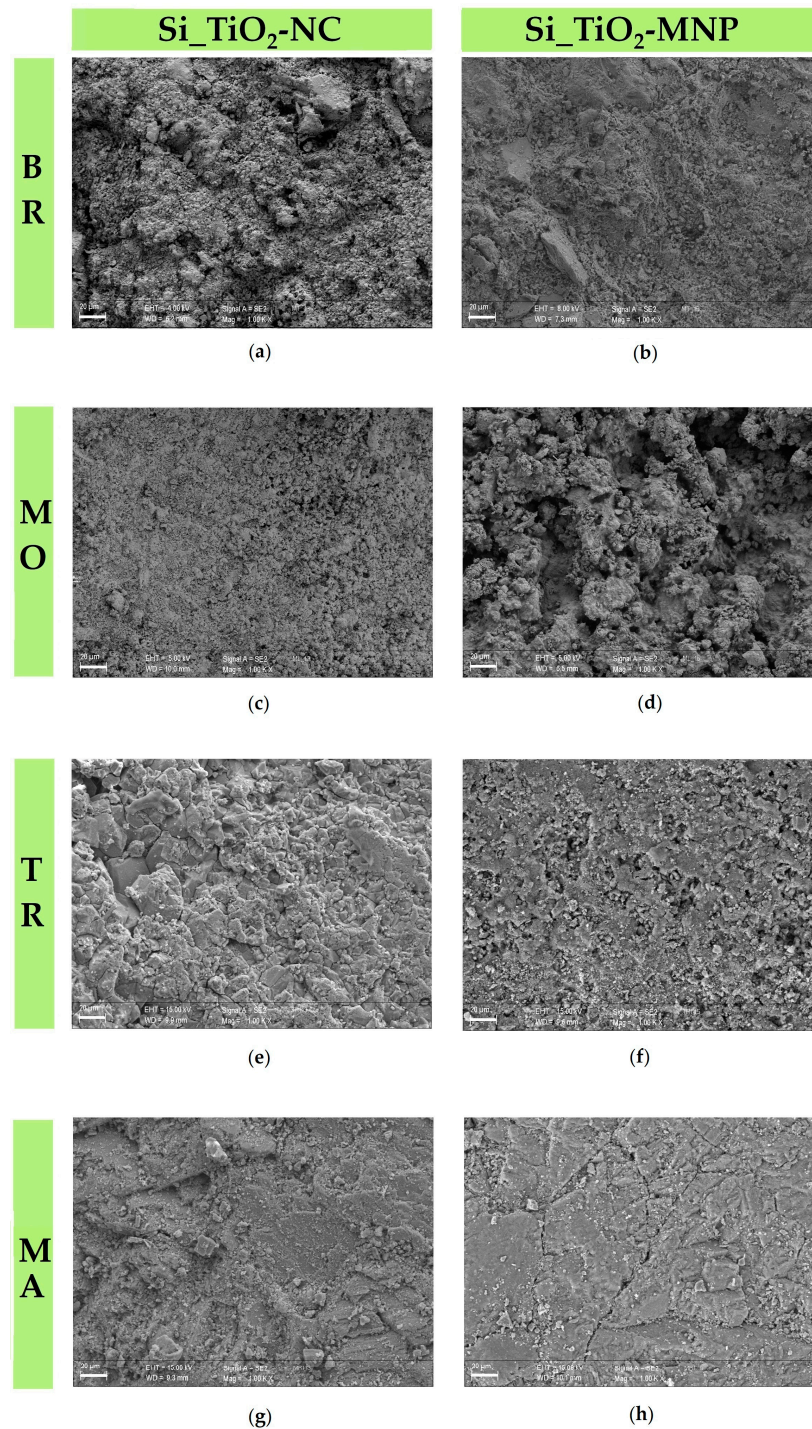


**Figure 4.** SEM micrographs (1000 $\times$ ) of: brick (BR) (a,b), mortar (MO) (c,d), travertine (TR) (e,f) and Carrara marble (MA) (g,h). Si\_TiO<sub>2</sub>-NC, coating with TiO<sub>2</sub> nanoparticles and loaded silica nanocapsules; Si\_TiO<sub>2</sub>-MNP, coating with TiO<sub>2</sub> nanoparticles and loaded silica mesoporous nanoparticles. Treated samples do not show cracks, despite nanoparticle aggregation evidences in some cases.

We analyzed the photo-degradation of methyl orange, used as a staining compound, dissolved in ethanol to allow quick evaporation of the liquid. The results, in terms of total color differences ( $\Delta E^*$ ) under UV light and natural light, are reported in Figure 5 and Figure S5 (Supplementary Materials), respectively. Here, we will comment in detail only on the laboratory results, since those obtained in-situ provide the same global information,

although with larger uncertainties and fluctuations, due to the uncontrolled environmental parameters and to the relatively short time of the investigation

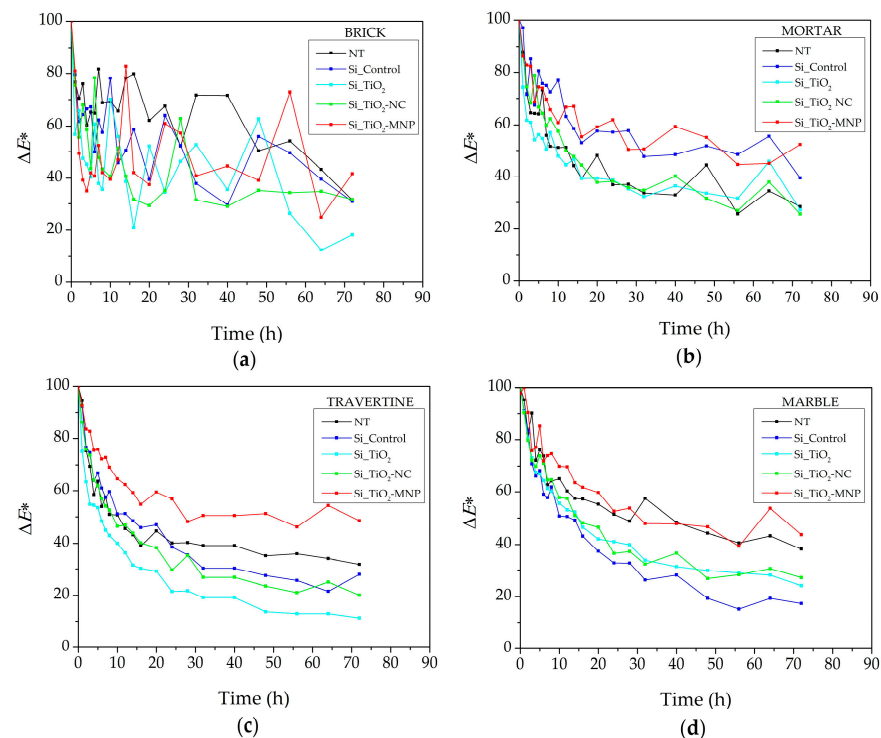


**Figure 5.** Evolution of total color difference ( $\Delta E^*$ ) for samples irradiated under UV light (365 nm) in laboratory conditions: (a) brick, (b) mortar, (c) travertine, and (d) Carrara marble. NT: untreated; Si\_Control: coating without nanoparticles; Si\_TiO<sub>2</sub>: coating with TiO<sub>2</sub> nanoparticles; Si\_TiO<sub>2</sub>-NC: coating with TiO<sub>2</sub> nanoparticles and loaded silica nanocapsules; Si\_TiO<sub>2</sub>-MNP: coating with TiO<sub>2</sub> nanoparticles and loaded silica mesoporous nanoparticles.

A discoloration effect was observed in all analyzed samples, although with different accuracy and intensity. In particular, we noticed that the larger fluctuations of  $\Delta E^*$  were observed in the case of brick: this was due to the low difference between the color of this material and that of the utilized dye. However, in this case, we noticed that, within the first few hours of exposition to the UV radiation,  $\Delta E^*$  decreased by 40% and slowly and noisily went to  $\Delta E^* = 40$  within the 72 h of observation. Looking at Figure 5b–d, we noticed that in all cases, the Si\_TiO<sub>2</sub>-MNP coating showed the worst performance. This might be due to the entrapment of TiO<sub>2</sub> nanoparticles within the MNP nanoparticles, preventing the right contact between TiO<sub>2</sub> nanoparticles and methyl orange. More importantly, we observed that all other coatings showed the same  $\Delta E^*$  exponential time dependence, with a characteristic time of about 10 h. These results confirm that the quantity of TiO<sub>2</sub> nanoparticles dispersed in the coating formulations is adequate to induce a photocatalytic effect.

#### 4. Conclusions

In this paper, we reported the chemico-physical characterization of novel multifunctional nanoparticle coatings suitable for application on stone materials of cultural heritage interest. Two different silica nanocontainers, namely NC and MNP, with different shapes and dimensions, and loaded with a commercial biocide, were dispersed, along with TiO<sub>2</sub> nanoparticles, in a TEOS based-coating. After treatment, all surfaces acquired waterproof properties, leading to a strong reduction of capillary water absorption coefficient; this was particularly true for brick and mortar. In addition, the natural behavior of the stones in terms of water vapor transmission rate, was not significantly affected. All coatings appeared uniformly distributed on the stone surfaces and did not cause optical variations

visible to the naked eyes. All treatments did not penetrate deeply in the stones; thus, remaining at the surfaces, where they exploited a protective function. We also verified that the concentration of TiO<sub>2</sub> nanoparticles used in the proposed formulations was sufficient to induce a photocatalytic function in most of the tested coatings. All of the obtained results demonstrate that the studied coatings are multifunctional. In fact, they present more than two relevant surface properties [33]: in-vitro antifouling capability, as shown in reference [11], and water repellency and photocatalytic properties, as demonstrated in the present manuscript. Moreover, in-situ antifouling tests are currently ongoing and we are close to a one-year long observation.

**Supplementary Materials:** The following are available online at <https://www.mdpi.com/article/10.3390/coatings11040480/s1>, Figure S1: Comparison of average  $R_z$  measured before and after treatment for the different studied materials. NT: untreated; Si\_Control: coating without nanoparticles; Si\_TiO<sub>2</sub>-NC: coating with TiO<sub>2</sub> nanoparticles and loaded silica nanocapsules; Si\_TiO<sub>2</sub>-MNP: coating with TiO<sub>2</sub> nanoparticles and loaded silica mesoporous nanoparticles, Figure S2: Ti distribution resulting from EDS-XFR mapping: (a) Si\_TiO<sub>2</sub>-NC on brick, (b) Si\_TiO<sub>2</sub>-MNP on brick, (c) Si\_TiO<sub>2</sub>-NC on mortar and (d) Si-TiO<sub>2</sub>-MNP on mortar, Figure S3: Si distribution resulting from EDS-XFR mapping: (a) Si\_TiO<sub>2</sub>-NC on travertine, (b) Si\_TiO<sub>2</sub>-MNP on travertine, (c) Si\_TiO<sub>2</sub>-NC on Carrara marble and (d) Si-TiO<sub>2</sub>-MNP on Carrara marble, Figure S4: SEM micrographs (1000×) of: Brick (BR) (a,b), mortar (MO) (c,d), travertine (TR) (e,f) and Carrara marble (MA) (g,h). NT: untreated; Si\_Control, coating without nanoparticles, Figure S5: Evolution of total color difference ( $\Delta E^*$ ) for samples irradiated in-situ with natural solar light: (a) brick, (b) mortar, (c) travertine, and (d) Carrara marble. NT: untreated; Si\_Control: coating without nanoparticles; Si\_TiO<sub>2</sub>: coating with TiO<sub>2</sub> nanoparticles; Si\_TiO<sub>2</sub>-NC: coating with TiO<sub>2</sub> nanoparticles and loaded silica nanocapsules; Si\_TiO<sub>2</sub>-MNP: coating with TiO<sub>2</sub> nanoparticles and loaded silica mesoporous nanoparticles, Table S1: Amount of applied product calculated by weighting the specimens before and after the application of coatings, Table S2: Amount of dry matter retained after one week from the application for all samples treated with all coatings, Table S3: Colorimetric Coordinates  $L^*$ ,  $a^*$  and  $b^*$  generated by all coatings on all stone samples.

**Author Contributions:** M.Z. performed and analyzed all experiments and wrote the manuscript. M.Z. and L.R. planned the experimental procedure, synthesized the coatings, and performed photocatalysis experiment. M.A.R. and A.S. coordinated the project. G.D.V. selected the stone samples and coordinated the SEM measurements. E.B. was responsible for the LIME laboratory, coordinated and the contact angle and optical surface roughness measurements. All authors have read and agreed to the published version of the manuscript.

**Funding:** The authors acknowledge funding from Regione Lazio, Italy, within the “SUPERARE” project (No. F86C18000650005) financed in the call “Gruppi di Ricerca”. The Grant of Excellence Departments, MIUR (ARTICOLO 1, COMMI 314-337 LEGGE 232/2016) is also greatly acknowledged.

**Institutional Review Board Statement:** Not applicable.

**Informed Consent Statement:** Not applicable.

**Data Availability Statement:** The study does not report any data.

**Acknowledgments:** The authors acknowledge support from Daniele De Felicis, Riccardo Moscatelli, and Edoardo Rossi (Engineering department, Roma Tre University) for the contact angle and optical surface roughness measurements, and Sergio Lo Mastro for SEM analysis. The availability of the LIME laboratory (Roma Tre University, Rome, Italy) is also acknowledged.

**Conflicts of Interest:** The authors declare no conflict of interest.

## References

1. Vidal, F.; Vicente, R.; Mendes Silva, J. Review of environmental and air pollution impacts on built heritage: 10 questions on corrosion and soiling effects for urban intervention. *J. Cult. Herit.* **2019**, *37*, 273–295. [[CrossRef](#)]
2. Martínez-Martínez, J.; Benavente, D.; Gomez-Heras, M.; Marco-Castaño, L.; García-Del-Cura, M.Á. Non-linear decay of building stones during freeze-thaw weathering processes. *Constr. Build. Mater.* **2013**, *38*, 443–454. [[CrossRef](#)]
3. Cardell, C.; Delalieux, F.; Roumpopoulos, K.; Moropoulou, A.; Auger, F.; Van Grieken, R. Salt-induced decay in calcareous stone monuments and buildings in a marine environment in SW France. *Constr. Build. Mater.* **2003**, *17*, 165–179. [[CrossRef](#)]

4. Miller, A.Z.; Sanmartín, P.; Pereira-Pardo, L.; Dionísio, A.; Saiz-Jimenez, C.; Macedo, M.F.; Prieto, B. Bioreceptivity of building stones: A review. *Sci. Total Environ.* **2012**, *426*, 1–12. [[CrossRef](#)] [[PubMed](#)]
5. Scheerer, S.; Ortega-Morales, O.; Gaylarde, C. Microbial deterioration of stone monuments—An updated overview. *Adv. Appl. Microbiol.* **2009**, *66*, 97–139. [[CrossRef](#)]
6. Young, M.E.; Alakomi, H.L.; Fortune, I.; Gorbushina, A.A.; Krumbein, W.E.; Maxwell, I.; McCullagh, C.; Robertson, P.; Saarela, M.; Valero, J.; et al. Development of a biocidal treatment regime to inhibit biological growths on cultural heritage: BIODAM. *Environ. Geol.* **2008**, *56*, 631–641. [[CrossRef](#)]
7. Arai, T.; Harino, H.; Ohji, M. *Ecotoxicology of Antifouling Biocides*; Langston, W.J., Ed.; Springer: Berlin/Heidelberg, Germany, 2009.
8. Srinivasan, M.; Swain, G.W. Managing the use of copper-based antifouling paints. *Environ. Manag.* **2007**, *39*, 423–441. [[CrossRef](#)]
9. Imbesi, P.M.; Gohad, N.V.; Eller, M.J.; Orihuela, B.; Rittschof, D.; Schweikert, E.A.; Mount, A.S.; Wooley, K.L. Noradrenaline-functionalized hyperbranched fluoropolymer–poly(ethylene glycol) cross-linked networks as dual-mode, anti-biofouling coatings. *ACS Nano* **2012**, *6*, 1503–1512. [[CrossRef](#)]
10. Jämsä, S.; Mahlberg, R.; Holopainen, U.; Ropponen, J.; Savolainen, A.; Ritschkoff, A.C. Slow release of a biocidal agent from polymeric microcapsules for preventing biodeterioration. *Prog. Org. Coat.* **2013**, *76*, 269–276. [[CrossRef](#)]
11. Ruggiero, L.; Di Bartolomeo, E.; Gasperi, T.; Luisetto, I.; Talone, A.; Zurlo, F.; Peddis, D.; Ricci, M.A.; Sodo, A. Silica nanosystems for active antifouling protection: Nanocapsules and mesoporous nanoparticles in controlled release applications. *J. Alloys Compd.* **2019**, *798*, 144–148. [[CrossRef](#)]
12. Mardones, L.E.; Legnoverde, M.S.; Monzón, J.D.; Bellotti, N.; Basaldella, E.I. Increasing the effectiveness of a liquid biocide component used in antifungal waterborne paints by its encapsulation in mesoporous silicas. *Prog. Org. Coat.* **2019**, *134*, 145–152. [[CrossRef](#)]
13. Dresler, C.; Saladino, M.L.; Demirbag, C.; Caponetti, E.; Chillura Martino, D.F.; Alduina, R. Development of controlled release systems of biocides for the conservation of cultural heritage. *Int. Biodeterior. Biodegrad.* **2017**, *125*, 150–156. [[CrossRef](#)]
14. Jin, X.; Zhang, R.; Su, M.; Li, H.; Yue, X.; Qin, D.; Jiang, Z. Functionalization of halloysite nanotubes by enlargement and layer-by-layer assembly for controlled release of the fungicide iodopropynyl butylcarbamate. *RSC Adv.* **2019**, *9*, 42062–42070. [[CrossRef](#)]
15. Ruggiero, L.; Bartoli, F.; Fidanza, M.R.; Zurlo, F.; Marconi, E.; Gasperi, T.; Tuti, S.; Crociani, L.; Di Bartolomeo, E.; Caneva, G.; et al. Encapsulation of environmentally-friendly biocides in silica nanosystems for multifunctional coatings. *Appl. Surf. Sci.* **2020**, *514*, 145908. [[CrossRef](#)]
16. Salazar-Hernández, C.; Zárraga, R.; Alonso, S.; Sugita, S.; Calixto, S.; Cervantes, J. Effect of solvent type on polycondensation of TEOS catalyzed by DBTL as used for stone consolidation. *J. Sol-Gel Sci. Technol.* **2009**, *49*, 301–310. [[CrossRef](#)]
17. Mosquera, M.J.; Bejarano, M.; De la Rosa-Fox, N.; Esquivias, L. Producing crack-free colloid-polymer hybrid gels by tailoring porosity. *Langmuir* **2003**, *19*, 951–957. [[CrossRef](#)]
18. Angulo-Olais, R.; Illescas, J.F.; Aguilar-Pliego, J.; Vargas, C.A.; Haro-Pérez, C. Gel point determination of TEOS-based polymeric materials with application on conservation of cultural heritage buildings. *Adv. Condens. Matter Phys.* **2018**, *2018*, 5784352. [[CrossRef](#)]
19. Kapridaki, C.; Maravelaki-Kalaitzaki, P. TiO<sub>2</sub>-SiO<sub>2</sub>-PDMS nano-composite hydrophobic coating with self-cleaning properties for marble protection. *Prog. Org. Coat.* **2013**, *76*, 400–410. [[CrossRef](#)]
20. Pinho, L.; Elhaddad, F.; Facio, D.S.; Mosquera, M.J. A novel TiO<sub>2</sub>-SiO<sub>2</sub> nanocomposite converts a very friable stone into a self-cleaning building material. *Appl. Surf. Sci.* **2013**, *275*, 389–396. [[CrossRef](#)]
21. Pinho, L.; Mosquera, M.J. Photocatalytic activity of TiO<sub>2</sub>-SiO<sub>2</sub> nanocomposites applied to buildings: Influence of particle size and loading. *Appl. Catal. B Environ.* **2013**, *134–135*, 205–221. [[CrossRef](#)]
22. Ruggiero, L.; Fidanza, M.R.; Iorio, M.; Tortora, L.; Caneva, G.; Ricci, M.A.; Sodo, A. Synthesis and characterization of TEOS coating added with innovative antifouling silica nanocontainers and TiO<sub>2</sub> nanoparticles. *Frontiers (Boulder)* **2020**, *7*, 1–11. [[CrossRef](#)]
23. Xu, F.; Li, D.; Zhang, Q.; Zhang, H.; Xu, J. Effects of addition of colloidal silica particles on TEOS-based stone protection using n-octylamine as a catalyst. *Prog. Org. Coat.* **2012**, *75*, 429–434. [[CrossRef](#)]
24. Haake, S.; Simon, S.; Favaro, M. The bologna cocktail-evaluation of consolidation treatments on monuments in france and italy after 20 years on natural aging. In Proceedings of the 10th International Congress on Deterioration and Conservation of Stone, Stockholm, Sweden, 27 June–2 July 2004; pp. 423–430.
25. UNI EN 15801:2010 *Conservation of Cultural Property—Test Methods—Determination of Water Absorption by Capillarity*; Ente Nazionale Italiano di Unificazione (UNI): Milan, Italy, 2010.
26. DIN 52 615 *Testing of Thermal Insulating Material: Determination of Water Vapour Permeability of Construction and Insulating Materials*; Deutsches Institut für Normung E.V. (DIN): Berlin, Germany, 1987.
27. Greenspan, L. Humidity fixed points of binary saturated aqueous solutions. *J. Res. Natl. Bur. Stand. Sect. A Phys. Chem.* **1977**, *81A*, 89. [[CrossRef](#)]
28. *Normal 43/93 Misura Colorimetriche di Superfici Opache (Italian Normative on Stone Material-Colorimetric Measurement of Opaque Surfaces)*; Commissione Beni Culturali Uni Normal: Roma, Italy, 1993.
29. Delgado Rodrigues, J.; Grossi, A. Indicators and ratings for the compatibility assessment of conservation actions. *J. Cult. Herit.* **2007**, *8*, 32–43. [[CrossRef](#)]

30. Sasse, H.S.; Snethlage, R. Methods for the evaluation of stone conservation treatments. In *Report of Dahlem Workshop on Saving our Architectural Heritage, Berlin*; Baer, N.S., Snethlage, R., Eds.; John Wiley and Sons: Hoboken, NJ, USA, 1996; pp. 223–243.
31. Hobson, T. *Parameters and Definitions for Roundness and Surface Measurements*; Taylor Hobson Ltd.: Leicester, UK, 2000.
32. Cappelletti, G.; Fermo, P. *Hydrophobic and Superhydrophobic Coatings for Limestone and Marble Conservation*; Elsevier Ltd.: Amsterdam, The Netherlands, 2016; ISBN 9781782422839.
33. Esmeryan, K.D. Critical aspects in fabricating multifunctional super-nonwetable coatings exhibiting icephobic and anti-biofouling properties. *Coatings* **2021**, *11*, 339. [[CrossRef](#)]